Int J Adv Manuf Technol (2015) 77:2209–2219
DOI 10.1007/s00170-014-6635-4

ORIGINAL ARTICLE

Chip temperature and its effects on chip morphology, cutting forces, and surface roughness in high-speed face milling of hardened steel

Xiaobin Cui · Jingxia Guo · Jun Zhao · Yanyan Yan

Received: 11 July 2014 / Accepted: 23 November 2014 / Published online: 3 December 2014

Abstract Experimental investigation and finite element simulation of face milling AISI H13 steel with CBN tool were conducted in order to acquire thorough understanding of the chip temperature and its effects on chip morphology, cutting forces, and surface roughness. Cutting speeds adopted in the tests and simulations were in the range of 800 to 1,600 m/min. Axial depth of cut and material removal rate were set to be invariable for each cutting speed. The cutting parameter zones where relatively high chip temperature (zone "***H***"), long helix chip (zone "***L***"), lower resultant cutting force (zone "***R***"), and lower surface roughness (zone "***S***") arose were distinguished. The analysis results showed that the higher chip temperature in zone "***H***" led to higher ductility of the chip, resulting in the formation of long helix chip instead of short washer-shaped chip. The thermal softening effects induced by higher chip temperature in zone "***H***" led to lower cutting force and more stable cutting process which was beneficial for the better surface finish. Relatively high chip temperature, relatively low resultant cutting force, and relatively low surface roughness arose at the same time in cutting parameter zone "***R***".

Keywords Chip temperature · Chip morphology · Cutting forces · Surface roughness · Face milling · Hardened steel · CBN tool

X. Cui (✉) · Y. Yan
School of Mechanical and Power Engineering, Henan Polytechnic University, Jiaozuo 454003, People's Republic of China
e-mail: kokcxb@163.com

J. Guo
School of Energy Science and Engineering, Henan Polytechnic University, Jiaozuo 454003, People's Republic of China

J. Zhao
Key Laboratory of High Efficiency and Clean Mechanical Manufacture of MOE, School of Mechanical Engineering, Shandong University, Jinan 250061, People's Republic of China

1 Introduction

In 1931, Salomon [1] proposed the concept of high-speed cutting (HSC) by means of high-speed milling tests. With the developments of cutting tools and machine tools, HSC technology has advanced to be widely applied in the manufacturing of mould and dies in their hardened state. Because of the retention of strength to higher temperature than other tool materials, excellent abrasion resistance, and resistance to reaction with the ferrous work materials, the CBN tool material is preferred [2] in the machining of hardened steel.

Considerable amount of researches [3–13] have been conducted in turning of hardened steels with CBN tools. Much valuable information has been provided for the application of CBN tools by these previous works. Hard milling owns advantages such as reduction of machining costs and elimination of part distortion caused by heat treatment, and it can even be an alternative for the grinding process [14]. However, relatively few researches were conducted in the field of milling hardened steel with CBN tools.

Cutting performance of CBN tools in end milling of hardened steel was investigated by Okada et al. [15]. The resluts showed that the CBN tools can adequately be applied to high-speed hard milling. Koshy et al. [16] performed end milling of AISI D2 hardened steel (58 HRC) with a round CBN insert. It was found that acceptable tool life and good surface finish can be obtained, and fracture of the cutting edge is the main wear mechanism for CBN tools. Braghini and Coelho [17] studied the CBN tool wear in end milling of AISI D6 hardened steel (58 HRC) at low/medium cutting speeds. It was reported that the CBN tools were capable of producing Ra values in the range of those obtained with surface grinding. The governing wear mechanism of the CBN tools was a combination of adhesion and abrasion. Aslan [18] conducted researches on performance and wear behavior of different cutting tools in

end milling of X210 Cr12 cold work tool steel (62 HRC). It was found that, when CBN tools were used, the best cutting performance can be achieved in terms of flank wear and surface finish. Increasingly high cutting speed has been adopted in the industries in order to maintain competitiveness. However, it can be concluded that cutting speeds adopted in these previous researches were limited, and few researches were conducted with cutting speeds higher than 800 m/min. These previous studies mainly concentrated on cutting performance and tool wear in end milling of hardened steel. Few studies were performed in the field of face milling of hardened steel to study chip morphology and cutting forces.

The cutting temperature has great effect on chip morphology, cutting forces, and surface roughness in machining of hardened steel. Therefore, it is essential to have thorough understanding of the variation of cutting temperature in the milling process. The Salomon curve [1] indicated that the cutting temperature may decrease as the cutting speed increases. However, it was concluded by Longbottom and Lanham [19] that the Salomon curve might not be valid for describing the tool–work interface temperature. This means, according to most of the previous studies, increment of cutting speed might not lead to reduction of cutting temperature. Milling is a typical interrupted cutting process widely applied to produce smooth surfaces with high geometric accuracy. There have been numerous experimental and theoretical researches on cutting temperature in interrupted cutting especially milling [20–24]. However, few studies were conducted in the field of face milling. Stephenson and Ali [20] studied both theoretically and experimentally the cutting temperatures in interrupted cutting. The theoretical results were compared with the cutting temperature measured through infrared and tool–chip thermocouple technique. It was reported without direct experimental support by Palmai [21] that, in contrast to continuous cutting, the temperature in interrupted cutting might decrease as the cutting speed increases. A numerical model was established by Lazoglu and Altintas [22] using the finite difference method in order to investigate the tool and chip temperature fields in continuous machining and time-varying milling process. It was found that there was good agreement between simulated temperature and the measured results. An infrared radiation pyrometer with two optical fibers were developed by Sato et al. [23] to measure the tool–chip interface temperature in end milling with binderless CBN tool. The temperature of the flank face of a cutting tool in high-speed milling was experimentally investigated by Ueda et al. [24] via a two-color pyrometer with an optical fiber.

Experimental investigation and finite element simulation of high-speed face milling of AISI H13 steel (46–47 HRC) with CBN tool are conducted in the present study. Cutting speeds ranging from 800 to 1,600 m/min are adopted in this work. Axial depth of cut is fixed and the material removal rate is invariable for each cutting speed used in the tests. Different combinations of radial depth of cut and feed per tooth are applied at each cutting speed. The variations of chip temperature are explored for each cutting speed. The effects of the chip temperature variations on chip morphology, cutting forces, and surface roughness are analyzed. The optimum cutting conditions are distinguished for different cutting speeds in terms of cutting forces and surface roughness.

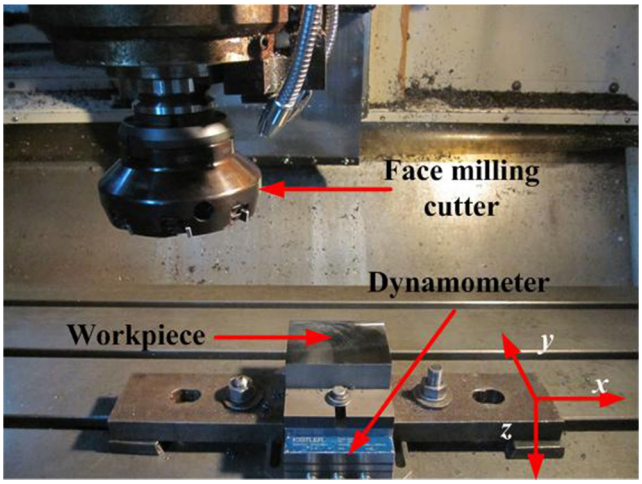

Fig. 1 The experimental setup for face milling test

2 Experimental procedures and finite element simulation

2.1 Cutting inserts and workpiece material

In the present study, tool holder with a tool diameter of 125 mm, major cutting edge angle of 75°, axial rake angle of −6°, and radial rake angle of −7° was used. The tool holder was capable of carrying eight inserts. CBN inserts were adopted in the milling tests. The milling tests were conducted on a vertical CNC machining center DAEWOO ACE-V500 without cutting fluid as shown in Fig. 1. The machining center with a 15 kW drive motor had a maximum spindle rotational speed of 10,000 rpm.

Since AISI H13 tool steel has great high-temperature strength and wear resistance, it has been widely applied in extrusion, hot forging, and pressure die casting. A block of AISI H13 steel (hardened to 46 to 47 HRC) was used in the present study. The width and length of it were 75 and 100 mm, respectively.

Table 1 Combinations (C) of a_e and f_z used at each cutting speed v

Cutting parameter	C1	C2	C3	C4	C5
a_e (mm)	15	30	45	60	75
f_z (mm/tooth)	0.24	0.12	0.08	0.06	0.048

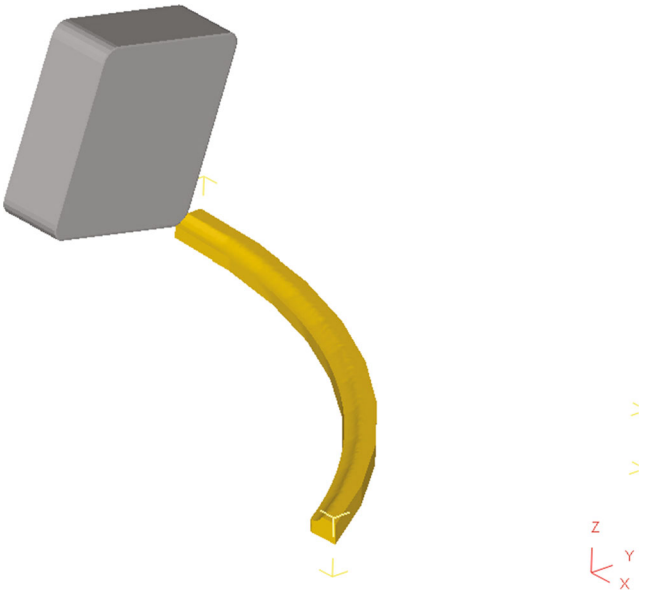

Fig. 2 Typical geometries of the workpiece and the cutting tool

2.2 Cutting tests

Up milling was applied in the tests according to the recommendation of the tool supplier. Since axial depth of cut a_p is mainly determined by process requirements, it was fixed as 0.2 mm in all the milling tests. Cutting speeds v ranging from 800 to 1,600 m/min at an interval of 200 m/min were used in the milling tests. The material removal rate was invariable for each cutting speed. Radial depth of cut a_e was in the range of 15 to 75 mm and feed per tooth f_z was in the range of 0.24 to 0.048 mm/tooth correspondingly as shown in Table 1.

For each combination of cutting parameters, fresh tools were used and each test was repeated three times. The cutting forces were measured using a Kistler piezoelectric dynamometer mounted on the machine table as shown in Fig. 1. The charge generated at the dynamometer was amplified by means of a multi-channel charge amplifier. The Sampling frequency of data is 10,000 Hz. After one pass of the workpiece surface, the surface roughness was measured using a portable surface roughness tester (Model TR200, China). The tool flank wear was observed by means of a digital microscope. The chip was analyzed using scanning electron microscopy (SEM) and energy dispersive X-ray spectroscopy (EDS).

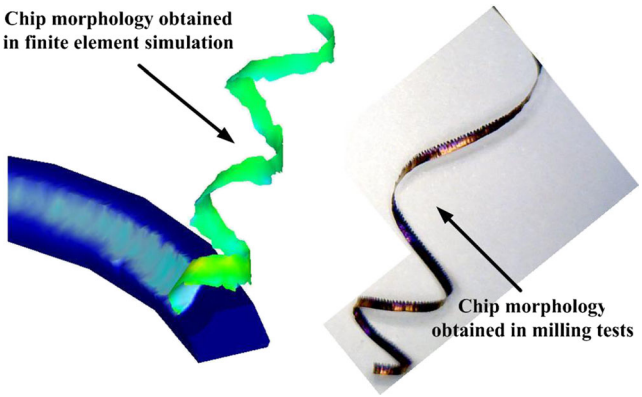

Fig. 3 Typical chip morphologies obtained in finite element simulation and milling tests (v=1,200 m/min, a_p=0.2 mm, f_z=0.08 mm/tooth, a_e= 45 mm)

2.3 Finite element simulation

Finite element method has been widely used to investigate quantities difficult to measure in the cutting process. Since the intensity and area of the heat source keep changing with the rotation of the cutting tool, there exists great difficulty in measuring the chip temperature directly in the milling process. Therefore, finite element simulation of face milling was conducted in the present study to analyze the variation of chip temperature.

Lagrangian formulation which was embedded in the Deform 3D package was used in the simulation. Figure 2 shows the typical geometries of the workpiece and the cutting tool. The geometry of the workpiece was simplified in order to enhance the simulation efficiency. The boundary conditions of the workpiece were set to restrict the bottom surface in lateral and vertical directions. The top surface of the cutting tool was constrained in vertical directions according to the actual milling condition. The cutting tool was also set to rotate at the specified cutting speed. The initial temperatures of the workpiece and cutter were 20 °C. Tetrahedron elements were utilized in the meshing of the workpiece and the cutter. Remeshing and local refining technology were employed for the meshing of the workpiece.

Table 2 shows the material properties of the workpiece and the cutting tool. It is essential for successfully simulating the cutting process to use a proper material-constitutive model for the workpiece. The Johnson-Cook model has been

Table 2 Material properties of the workpiece and the cutting tool

	Density (kg m^{-3})	Young's modulus (GPa)	Poisson ratio	Specific heat (Jkg^{-1} K^{-1})	Thermal conductivity (W m^{-1} K^{-1})	Thermal expansion (10^{-6} K^{-1})
Workpiece	7,780	208	0.27	560	28.40	10.40
Cutting tool	4,340	582	0.15	750	43	4.70

extensively used to study the deformation behavior of the workpiece in the cutting process. The Johnson-Cook constitutive equation can be expressed as:

$$\overline{\sigma} = \left[A + B\left(\overline{\varepsilon}\right)^{n}\right]\left[1 + C\ln\left(\frac{\overline{\varepsilon}}{\overline{\varepsilon_0}}\right)\right]\left[1-\left(\frac{T_a - T_r}{T_m - T_r}\right)^{m}\right] \quad (1)$$

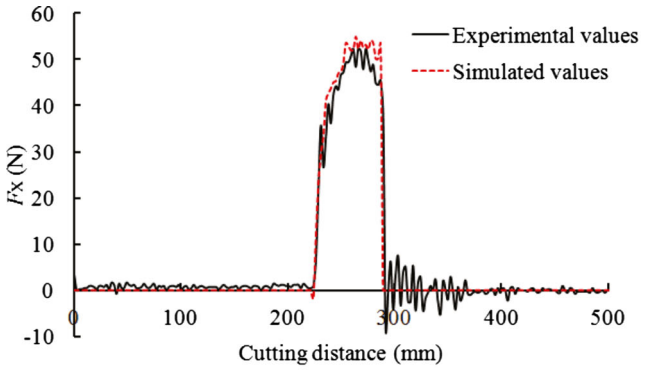

(a) Cutting force F_x obtained in direction X

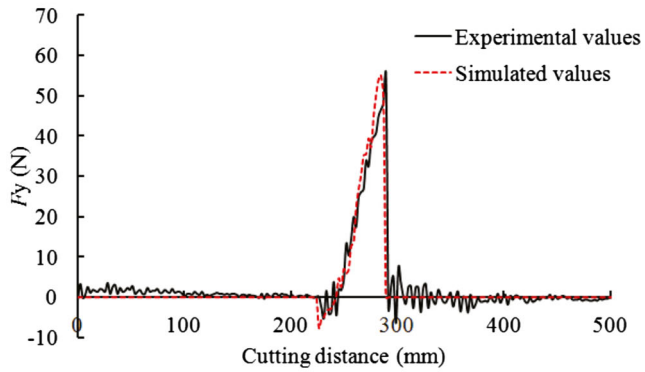

(b) Cutting force F_y obtained in direction Y

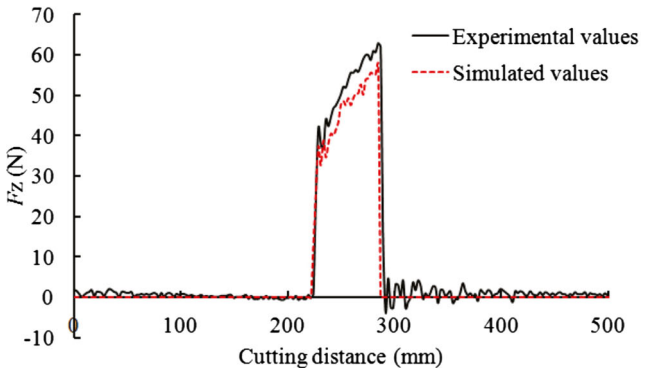

(c) Cutting force F_z obtained in direction Z

Fig. 4 Cutting forces obtained in finite element simulation and milling tests (v=1,200 m/min, a_p=0.2 mm, f_z=0.08 mm/tooth, a_e=45 mm). **a** Cutting force F_x obtained in direction X. **b** Cutting force F_y obtained in direction Y. **c** Cutting force F_z obtained in direction Z

where $\overline{\sigma}$, $\overline{\varepsilon}$, $\dot{\overline{\varepsilon}}$ and T_a are the shear stress, shear strain, shear strain rate, and absolute temperature, respectively. The material properties are determined by the yield strength A, the hardening modulus B, the reference plastic strain $\overline{\varepsilon_0}$, the strain rate sensitivity C, the strain hardening exponent n, the thermal softening coefficient m, the reference temperature T_r, and the melting temperature T_m. According to the work by Chen et al. [25], these Johnson-Cook parameters can be set as A=715 MPa, B=329 MPa, C=0.03, n=0.28, and m=1.5.

3 Results and discussion

3.1 Chip temperature

It has been mentioned that the increment of cutting speed might not lead to reduction of cutting temperature according to the work by Longbottom and Lanham [19]. Taking this into consideration, the variations of chip temperature induced by different combinations of radial depth of cut and feed per tooth were analyzed for each cutting speed in the present study.

Chip morphologies and cutting forces acquired from the finite element simulation and milling tests were compared. It was found that there was good consistency between the simulated and experimental results. Typical morphologies of the chip were shown in Fig. 3. It can be seen that these chip shared similar geometric characteristics. Figure 4 shows the comparison between the simulated and experimental cutting forces for typical combination of cutting parameters. Cutting forces in three directions X, Y, and Z were represented by F_x, F_y, and F_z, respectively. It can be seen from Fig. 4 that the simulated and experimental values were close to each other. Comparison of the chip morphologies and cutting forces between the simulated and experimental results validated the correctness of the simulation.

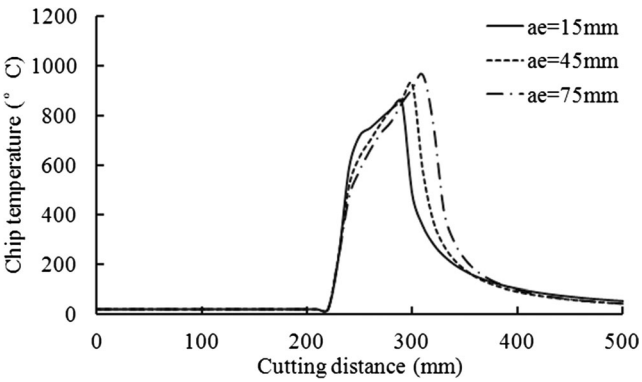

Fig. 5 Development of chip temperature with cutting distance for different combinations of cutting parameters (v=1,200 m/min, a_p=0.2 mm)

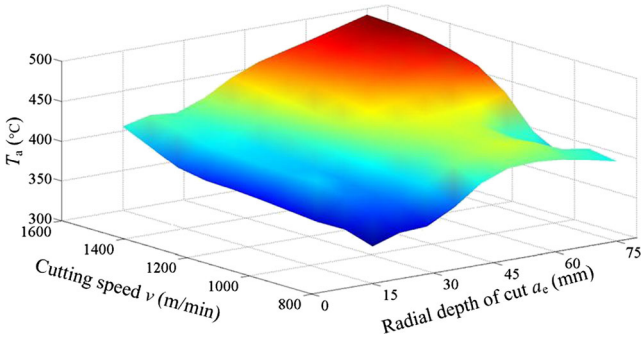

Fig. 6 Fitted curved surface for chip temperature T_a obtained under different cutting parameter combinations

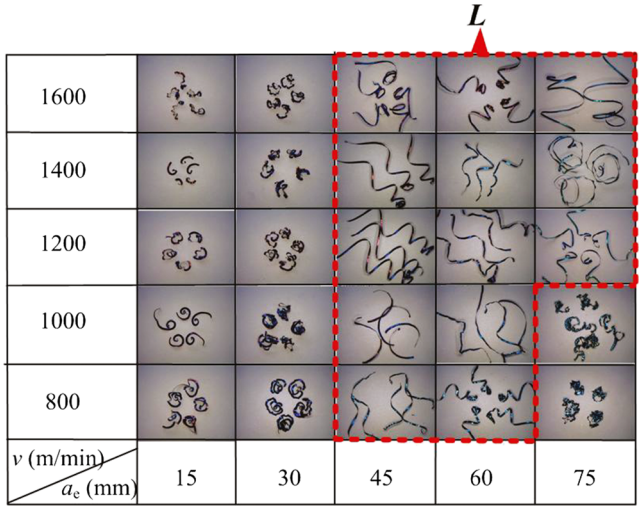

Fig. 8 The evolution of chip morphology with cutting speed v and radial depth of cut a_e

The chip temperature was influenced greatly by factors such as intensity, area, and duration of the heat source. When varying combinations of cutting parameters are applied, these influencing factors will evolve in different ways with tool rotation. It was found that, although the axial depth of cut, cutting speed, and metal removal rate were fixed, the chip temperature varied for different combinations of radial depth of cut and feed per tooth. Taking the cutting speed of 1,200 m/min as an example, the development of the highest temperature on the chip with cutting distance for different combination of cutting parameters are presented in Fig. 5. It can be seen from Fig. 5 that the evolution trends of the chip temperature exhibited similar characteristics for different values of radial depth of cut. In the cutting period, the rising rate of the chip temperature decreased with the increment of the chip temperature. The chip temperature decreased rapidly after the cutting tool left the workpiece. It was found that, at the cutting speed of 1,200 m/min, the peak value of the chip temperature increased as the radial depth of cut increased from 15 to 75 mm.

The average values of the chip temperature T_a were calculated for the cutting period. Figure 6 shows the fitted curved surface for chip temperature T_a obtained under different cutting parameter combinations. It can be seen that the chip temperature increased with the increment of the cutting speed at each radial depth of cut. The evolution trends of the chip temperature with radial depth of cut differed for different values of cutting speed. At cutting speeds of 800 and 1,000 m/min, the chip temperature first increased with the radial depth of cut and then decreased. Higher chip temperature arose when the radial depth of cut was in the range of 30 mm$<a_e<$75 mm. When the cutting speed was higher than 1,000 m/min, the chip temperature kept increasing as the radial depth of cut increased from 15 to 75 mm. Relatively high chip temperature appeared when the radial depth of cut was higher than 30 mm. Figure 7 shows the contour map of chip temperature T_a with cutting speed v and radial depth of

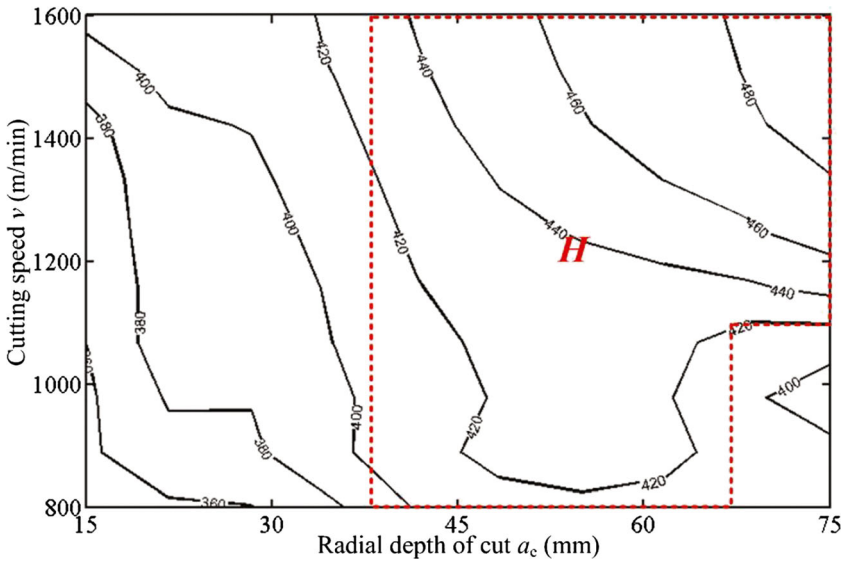

Fig. 7 Contour map of chip temperature T_a (degress Celsius) with cutting speed v and radial depth of cut a_e

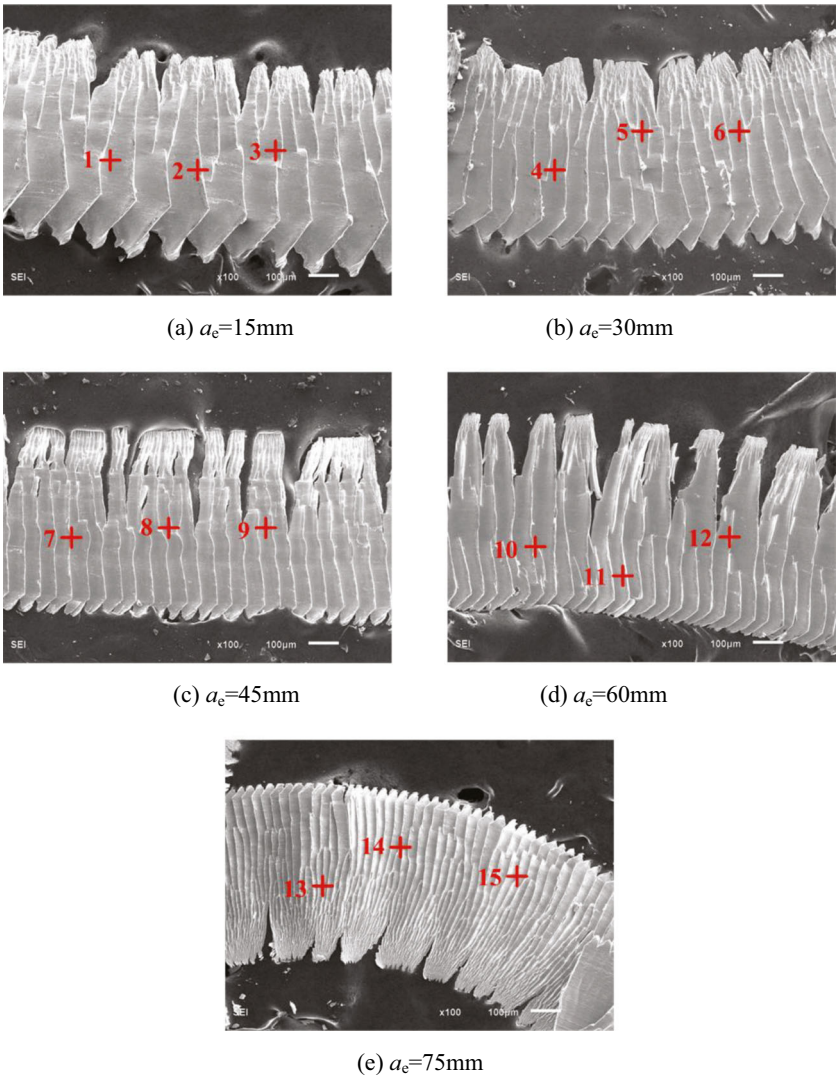

(a) a_e=15mm (b) a_e=30mm

(c) a_e=45mm (d) a_e=60mm

(e) a_e=75mm

Fig. 9 Typical magnified chip morphologies obtained at different radial depth of cut a_e (v= 1,200 m/min, a_p=0.2 mm). **a** a_e= 15, **b** a_e=30, **c** a_e=45, **d** a_e=60, **e** a_e=75 mm

cut a_e. It can be seen that relatively high chip temperature arose in cutting parameter zone "***H***" denoted in Fig. 7.

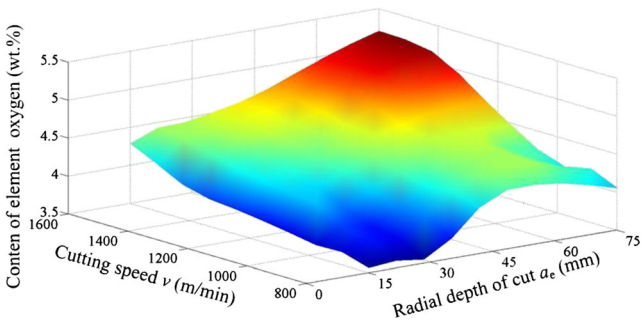

Fig. 10 Fitted curved surface for content of element oxygen on the chip obtained under different cutting parameter combinations

3.2 Chip morphology

Figure 8 shows the evolution of chip morphology with cutting speed v and radial depth of cut a_e. It can be seen that the chip morphology exhibited varying characteristics even at the same cutting speed. Generally, two kinds of chip morphology, namely short washer-shaped chip and long helix chip, arose in the cutting process. At cutting speeds of 800 and 1,000 m/min, short washer-shaped chip formed when the radial depth of cut was relatively small (15 and 30 mm) or large (75 mm). Long helix chip appeared when the other values of radial depth of cut (45 and 60 mm) were applied. When cutting speed was in the range of 1,200 to 1,600 m/min, the characteristics of chip morphology appeared to be similar to that obtained at cutting speeds of 800 and 1,000 m/min, except for that long helix chip arose when the radial depth of cut was 75 mm. The cutting parameter zone where long helix chip formed was denoted as "***L***" as shown in Fig. 7.

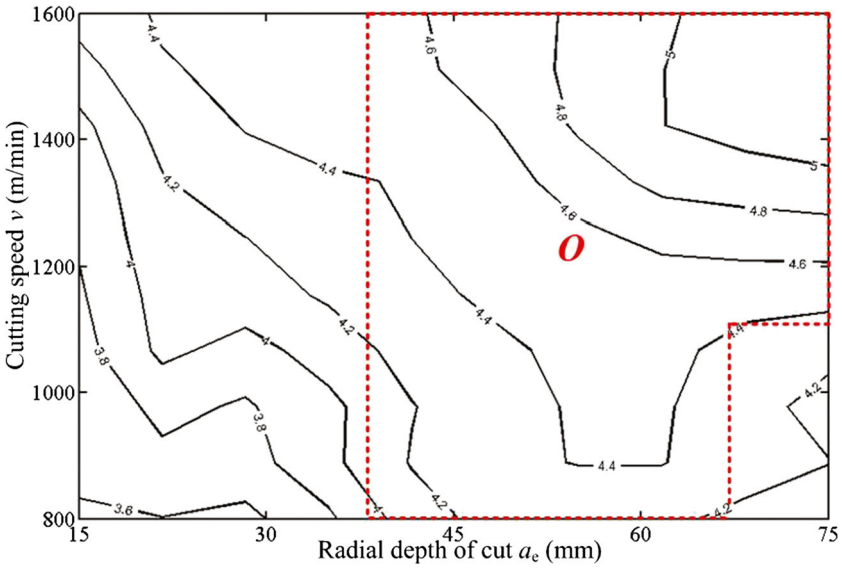

Fig. 11 Contour map of content of element oxygen (weight percent) with cutting speed v and radial depth of cut a_e

Comparisons between zone "***H***" and zone "***L***" in Fig. 7 were conducted, and it was found that these two zones represented the similar combinations of cutting parameters. The cutting temperature had great influence on chip formation. When the ductility of the workpiece material was high, it was more difficult for chip breaking to happen, and long helix chip was more likely to appear. It has been discussed that relatively high chip temperature arose in zone "***L***." The higher chip temperature caused higher ductility of the chip, leading to the formation of long helix chip instead of short washer-shaped chip.

In the present work, the middle part of the chip obtained in the milling process was analyzed using SEM and EDS. Three EDS analyses were conducted for each chip. The average value of the content of element oxygen was calculated. It was found that, for different cutting speeds, the magnified chip morphology obtained using SEM exhibited similar trends as the radial depth of cut increased. Considering the cutting speed of 1,200 m/min as an example, the typical magnified chip morphologies obtained at different radial depth of cut is shown in Fig. 9. It can be seen from Fig. 9 that the segment spacing of the chip decreased with the increment of the radial depth of cut. For the purpose of maintaining the metal removal rate, the feed per tooth (the average value of the uncut chip thickness) was reduced as the radial depth of cut increased for each cutting speed. The decreasing trend of segment spacing was consistent with the work by Davies et al. [26]. It was stated by Davies et al. [26] that the segment spacing decreased with the reduction of uncut chip thickness.

Figure 10 presents the fitted curved surface for the content of element oxygen on the chip obtained under different cutting parameter combinations. It was found that the evolution of content of element oxygen with cutting speed and radial depth of cut was similar to that of chip temperature. With the increment of the cutting speed, the content of element oxygen increased for each radial depth of cut. The content increased first and then decreased with the radial depth of cut at cutting speeds of 800 and 1,000 m/min. As the cutting speed increased over 1,000 m/min, the content increased with the increment of radial depth of cut. Figure 11 shows the contour map of content of element oxygen with cutting speed v and radial depth of cut a_e. It can be seen from the cutting parameter zone "***O***" denoted in Fig. 11 that higher content of element oxygen appeared. Cutting parameter combinations in zone

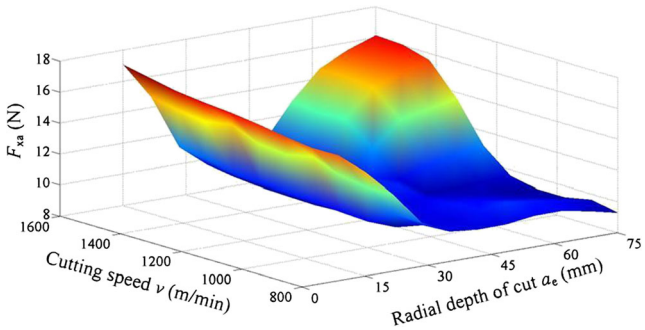

Fig. 12 Fitted curved surface for F_{xa} obtained under different cutting parameter combinations

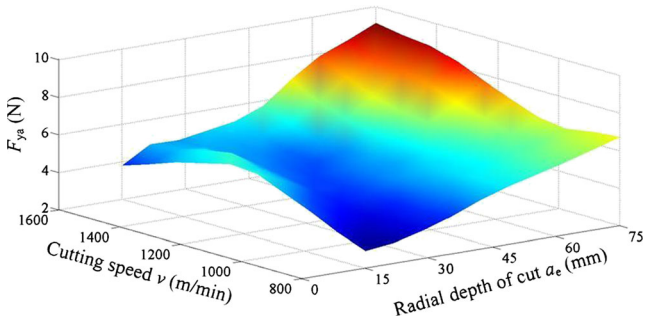

Fig. 13 Fitted curved surface for F_{ya} obtained under different cutting parameter combinations

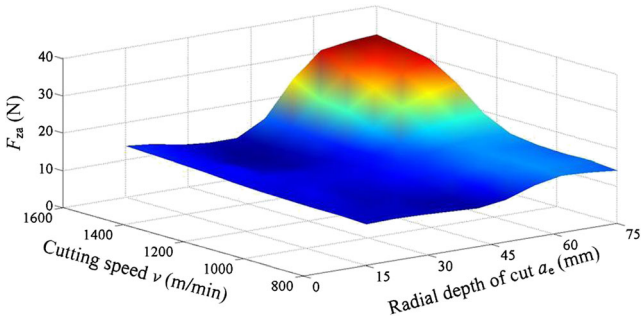

Fig. 14 Fitted curved surface for F_{za} obtained under different cutting parameter combinations

"***O***" was consistent with those in zone "***H***" in Fig. 7. The higher chip temperature which arose in the cutting process accelerated the chemical reaction between the elements iron in the workpiece and oxygen in the air, resulting in higher content of element oxygen on the chip. This should be the main reason why evolving trends of content of element oxygen on the chip is analogous to that of chip temperature.

3.3 Cutting forces

For each combination of cutting parameters, the cutting forces were recorded when the milling cutter arrive at the position where the radial depth of cut a_e listed in Table 1 was reached. Three cutting cycles were picked for each trial. The average values of the cutting forces in three directions X, Y, and Z were calculated, and they were represented by F_{xa}, F_{ya}, and F_{za}, respectively. The data points of the resultant cutting force F_{ri} can be obtained by means of Eq. 1:

$$F_{ri} = \sqrt{{F_{xi}}^2 + {F_{yi}}^2 + {F_{zi}}^2} \tag{1}$$

where F_{xi}, F_{yi}, and F_{zi} were data points of the cutting forces in directions X, Y, and Z, respectively. F_{ra} was used to represent the average value of the resultant cutting force F_{ri}.

Figures 12, 13, and 14 show the fitted curved surface for cutting forces F_{xa}, F_{ya}, and F_{za} obtained under different cutting parameter combinations. It was found that the cutting parameter zone where relatively low cutting force arose differed for different directions. When the cutting speed was no more than 1,200 m/min, radial depth of cut above 30 mm should be used so as to acquire relatively low value of F_{xa}. At cutting speeds higher than 1,200 m/min, relatively low F_{xa} can be obtained when radial depth of cut was in the range of 30 to 45 mm. For the purpose of acquiring relatively low value of F_{ya}, cutting speeds ranging from 800 to 1,000 m/min should be applied, and radial depth should be in the range of 15 to 30 mm. Radial depth of cut lower than 45 mm should be used in order to obtain relatively low F_{za}.

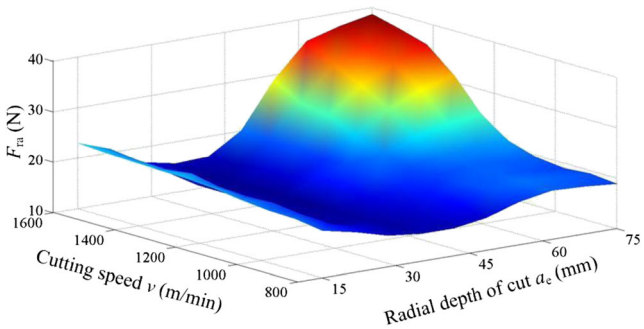

Fig. 15 Fitted curved surface for F_{ra} obtained under different cutting parameter combinations

Figure 15 shows fitted curved surface for resultant cutting force F_{ra} obtained under different cutting parameter combinations. It can be seen from Fig. 15 that F_{ra} decreased first and then increased with a_e for each cutting speed used in the present work. When the cutting speed was below 1,000 m/min, radial depth of cut above 30 mm and below 75 mm should be applied in order to obtain relatively low value of F_{ra}. However, radial depth of cut close to 45 mm should be adopted when the cutting speed increased over 1,000 m/min. Figure 16 shows the contour map of F_{ra} with cutting speed v and radial depth of cut a_e. Lower values of F_{ra} were located in the cutting parameter zone "***R***" shown in Fig. 16. Compared with zone "***H***" denoted in Fig. 7, the range of cutting parameters covered in zone "***R***" was narrower. It was found that the main difference between zone "***H***" and zone "***R***" was zone "***W***" denoted in Fig. 16. Figure 17 shows the contour map of tool wear after one pass of the workpiece surface with cutting speed v and radial depth of cut a_e. It was found from Fig. 17 that relatively high values of tool wear arose in cutting parameter zone "***W***" and higher cutting force existed in this zone. As has been discussed in "Section 3.1," for each cutting speed, though the metal removal rate was invariable, the chip temperature changed with different combinations of radial depth of cut a_e and feed per tooth f_z. Taking the thermal softening effects induced by higher chip temperature into account, relatively low values of resultant cutting forces were expected to appear in cutting parameter zone "***H***" denoted in Fig. 7. However, higher cutting temperature made the cutting tool softer and led to the higher values of tool wear in zone "***W***" which accelerated the friction between the cutting tool and workpiece, resulting in the higher values of resultant cutting forces in zone "***W***".

3.4 Surface roughness

For each combination of cutting parameters, surface roughness Ra was measured three times after the first pass of the workpiece surface, and the average value was calculated. Figure 18 shows the fitted curved surface for surface roughness Ra obtained under different cutting parameter combinations. It can be seen from Fig. 18 that, for each cutting speed, surface roughness generally decreased as the radial depth of

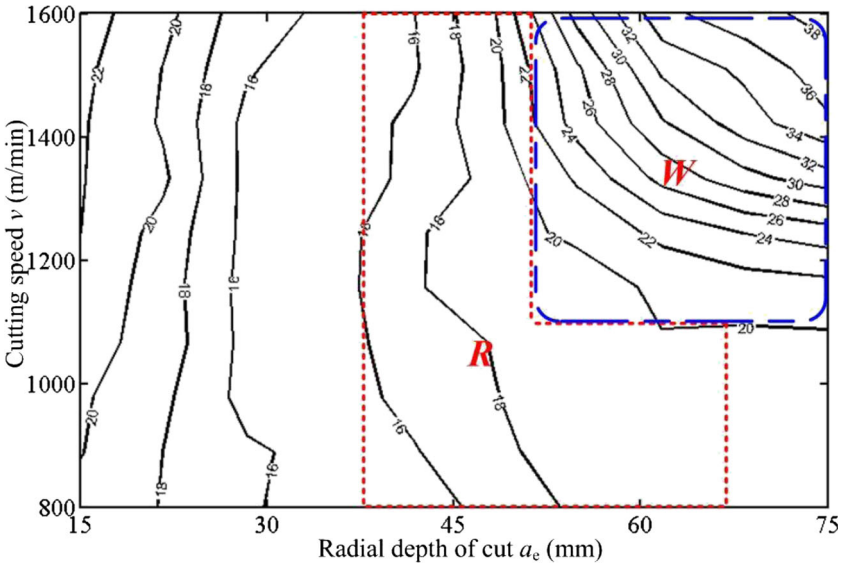

Fig. 16 Contour map of F_{ra} (Newton) with cutting speed v and radial depth of cut a_e

cut increased. It has been mentioned that the feed per tooth was set to decrease with the increment of radial depth of cut so that the material removal rate was constant. The decreasing trend of surface roughness can be attributed to the reduction of uncut chip thickness. When the cutting speed was no more than 1,000 m/min, radial depth of cut should be in the range of 30 mm$<a_e<$75 mm so that lower surface roughness can be obtained. Radial depth of cut above 30 mm should be used to obtain better surface finish as the cutting speed increased over 1,000 m/min. Contour map of surface roughness Ra (micrometers) with cutting speed v and radial depth of cut a_e was shown in Fig. 19. It was found that relatively good surface finish was more likely to arise in cutting parameter zone "***S***" denoted in Fig. 19. It can be seen that zone "***S***" is approximately the same to zone "***H***" in Fig. 7. The thermal softening effects induced by higher chip temperature led to lower cutting force and more stable cutting process. Therefore, it was inferred that the higher chip temperature contributed to the better surface finish in zone "***S***" to some extent. It should be noted that, though the tool wear was relatively high in cutting parameter zone "***W***", surface roughness obtained in zone "***W***" was relatively low. It seems that the tool wear in zone "***W***" which was lower than 0.06 mm had little effect on the surface roughness of the machined workpiece.

It can be concluded that relatively high chip temperature and relatively low values of resultant cutting force and surface roughness arose at the same time in cutting parameter zone "***R***" denoted in Fig. 16.

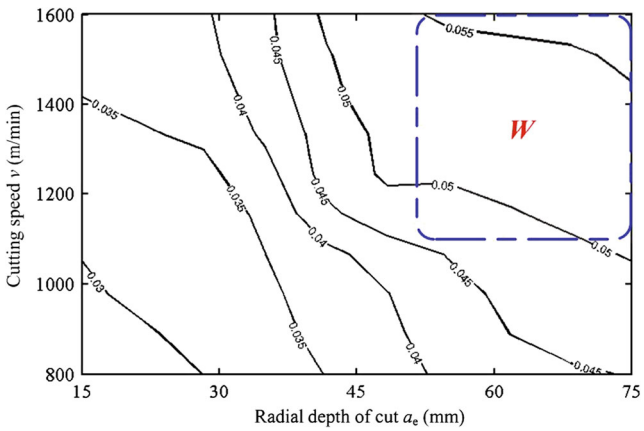

Fig. 17 Contour map of tool wear (millimeters) after one pass of the workpiece surface with cutting speed v and radial depth of cut a_e

4 Conclusions

In the present study, experimental investigation and finite element simulation of high-speed face milling of AISI H13 steel with CBN tool used was conducted in order to analyze chip temperature and its effects on chip morphology, cutting forces, and surface roughness. For each cutting speed adopted in this work, the metal removal rate is fixed. The following conclusions can be drawn from this work:

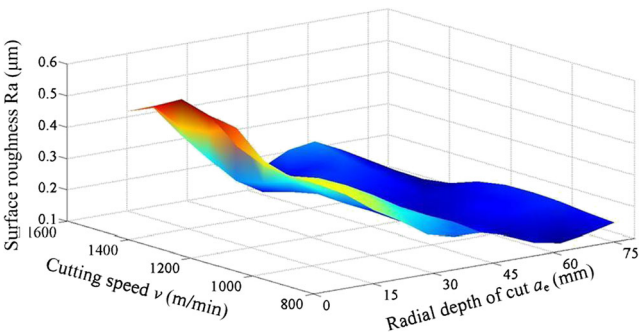

Fig. 18 Fitted curved surface for surface roughness Ra (micrometers) obtained under different cutting parameter combinations

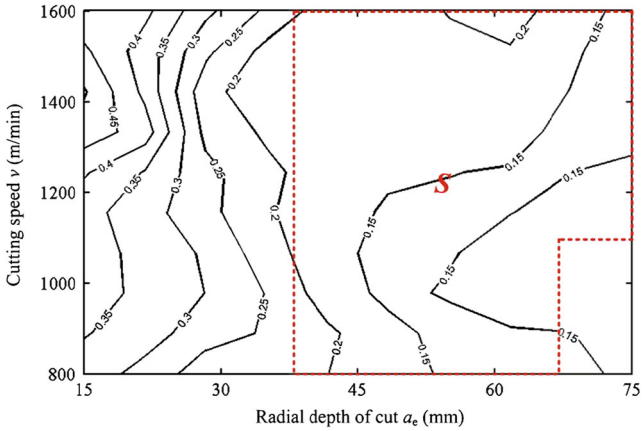

Fig. 19 Contour map of surface roughness Ra (micrometers) with cutting speed v and radial depth of cut a_e

1. Though the axial depth of cut, cutting speed, and metal removal rate were fixed, it was found that the chip temperature varied for different combinations of radial depth of cut and feed per tooth. For each combination of cutting parameters, the rising rate of the chip temperature decreases with the increment of the chip temperature in the cutting period. The chip temperature decreased rapidly after the cutting tool left the workpiece. At the cutting speeds of 800 m/min and 1,000 m/min, the chip temperature increased first as the radial depth of cut increased and then decreased. At cutting speeds higher than 1,000 m/min, the chip temperature kept increasing as the radial depth of cut increased from 15 to 75 mm. The cutting parameter zone "***H***" where relatively high chip temperature arose was identified in the present work.
2. The chip morphology exhibited varying characteristics even at the same cutting speed. The cutting parameter zone "***L***" where long helix chip formed was distinguished. Due to the higher chip temperature in cutting parameter zone "***H***" which caused higher ductility of the chip, long helix chip instead of short washer-shaped chip formed. Higher chip temperature in zone "***H***" accelerated the chemical reaction between the elements iron in the workpiece and oxygen in the air.
3. The cutting parameter zone where lower cutting force arose differed for different directions. It was found that the average value of the resultant cutting force F_{ra} decreased first and then increased with a_e for each cutting speed. The cutting parameter zone "***R***" where lower cutting force can be obtained was identified. The thermal softening effects induced by higher chip temperature had great effect on cutting forces. Relatively high values of tool wear arose in cutting parameter zone "***W***," resulting in higher cutting force in this zone.
4. Generally, surface roughness decreased with the increment of radial depth of cut for each cutting speed. The cutting parameter zone "***S***" where relatively good surface finish arose was identified. The thermal softening effects induced by higher chip temperature led to lower cutting force and more stable cutting process which was beneficial for the better surface finish in zone "***S***." Relatively high chip temperature, relatively low resultant cutting force and relatively low surface roughness arose at the same time in cutting parameter zone "***R***."

Acknowledgments This research is supported by the Doctor Foundation from Henan Polytechnic University (B2014-032), the National Natural Science Foundation of China (51175310), and the National Natural Science Foundation of China (51205112).

References

1. Salomon CJ (1931) Process for machining metals of similar acting materials when being worked by cutting tools. German patent, Number 523594
2. Trent EM, Wright PK (2000) Metal cutting, 4th edn. Butterworth-Heinemann, Woburn
3. Huang Y, Liang SY (2003) Cutting forces modeling considering the effect of tool thermal property-application to CBN hard turning. Int J Mach Tools Manuf 43(3):307–315
4. Huang Y, Liang SY (2005) Modeling of cutting forces under hard turning conditions considering tool wear effect. J Manuf Sci Eng Trans ASME 127(2):262–270
5. Benga GC, Abrao AM (2003) Turning of hardened 100Cr6 bearing steel with ceramic and PCBN cutting tools. J Mater Process Technol 143–144(1):237–241
6. Özel T, Hsu TK, Zeren E (2005) Effects of cutting edge geometry, workpiece hardness, feed rate and cutting speed on surface roughness and forces in finish turning of hardened AISI H13 steel. Int J Adv Manuf Technol 25(3–4):262–269
7. Arsecularatne JA, Zhang LC, Montross C, Mathew P (2006) On machining of hardened AISI D2 steel with PCBN tools. J Mater Process Technol 171(2):244–252
8. Halpin T, Byrne G, Barry J, Ahearne E (2009) The performance of polycrystalline cubic boron nitride tools in continuous, semi-interrupted, and interrupted hard machining. Proc IMechE B J Eng Manuf 223(8):947–953
9. Kishawy HA, Elbestawi MA (2001) Tool wear and surface integrity during high-speed turning of hardened steel with polycrystalline cubic boron nitride tools. Proc IMechE B J Eng Manuf 215(6): 755–767
10. Dureja JS, Gupta VK, Sharma VS, Dogra M (2010) Wear mechanisms of TiN-coated CBN tool during finish hard turning of hot tool die steel. Proc IMechE B J Eng Manuf 224(4):553–566
11. Chou YK, Evans CJ, Barash MM (2002) Experimental investigation on CBN turning of hardened AISI 52100 steel. J Mater Process Technol 124(3):274–283
12. Huang Y, Liang SY (2004) Modeling of CBN tool flank wear progression in finish hard turning. J Manuf Sci Eng Trans ASME 126(1):98–106
13. Huang Y, Liang SY (2004) Modelling of CBN tool crater wear in finish hard turning. Int J Adv Manuf Technol 24(9–10):632–639
14. Iqbal A, He N, Li L, Dar NU (2007) A fuzzy expert system for optimizing parameters and predicting performance measures in hard-milling process. Expert Syst Appl 32(4):1020–1027

15. Okada M, Hosokawa A, Tanaka R, Ueda T (2011) Cutting performance of PVD-coated carbide and CBN tools in hardmilling. Int J Mach Tools Manuf 51(2):127–132
16. Koshy P, Dewes RC, Aspinwall DK (2002) High speed end milling of hardened AISI D2 tool steel (~58 HRC). J Mater Process Technol 127(2):266–273
17. Braghini A, Coelho RT (2001) An investigation of the wear mechanisms of polycrystalline cubic boron nitride (PCBN) tools when end milling hardened steels at low/medium cutting speeds. Int J Adv Manuf Technol 17(4):244–251
18. Aslan E (2005) Experimental investigation of cutting tool performance in high speed cutting of hardened X210 Cr12 cold-work tool steel (62 HRC). Mater Des 26(1):21–27
19. Longbottom JM, Lanham JD (2006) A review of research related to Salomon's hypothesis on cutting speeds and temperatures. Int J Mach Tools Manuf 46(14):1740–1747
20. Stephenson DA, Ali A (1992) Tool temperatures in interrupted metal cutting. J Manuf Sci Eng Trans ASME 114(2):127–136
21. Palmai Z (1987) Cutting temperature in intermittent cutting. Int J Mach Tools Manuf 27(2):261–274
22. Lazoglu I, Altintas Y (2002) Prediction of tool and chip temperature in continuous and interrupted machining. Int J Mach Tools Manuf 42(9):1011–1022
23. Sato M, Ueda T, Tanaka H (2007) An experimental technique for the measurement of temperature on CBN tool face in end milling. Int J Mach Tools Manuf 47(14):2071–2076
24. Ueda T, Hosokawa A, Oda K, Yamada K (2001) Temperature on flank face of cutting tool in high speed milling. CIRP Ann Manuf Technol 50(1):37–40
25. Chen L, El-Wardany TI, Nasr M, Elbestawi MA (2006) Effects of edge preparation and feed when hard turning a hot work die steel with polycrystalline cubic boron nitride tools. CIRP Ann Manuf Technol 55(1):89–92
26. Davies MA, Chou Y, Evans CJ (1996) On chip morphology, tool wear and cutting mechanics in finish hard turning. CIRP Ann Manuf Technol 45(1):77–82